Progress In Electromagnetics Research M, Vol. 109, 217–229, 2022

Improved Three Vector Model Predictive Torque Control of PMSM

Qianghui Xiao[1], Zhe Li[1], Bing Luo[2], Tingting Wang[2], Dingdou Wen[1], and Yang Zhang[1, *]

Abstract—To reduce the computational complexity of traditional model predictive torque control (MPTC) and improve the sensitivity of predictive control to disturbances, an improved three vector model predictive control strategy applied in permanent magnet synchronous motor (PMSM) is proposed. First, the principle of deadbeat synchronization between torque and flux linkage is adopted to reduce six candidate vectors in traditional torque prediction to two, and the cost function is designed to select the optimal voltage vector. In addition, disturbance observation compensation is introduced to compensate for the influence of load disturbance on the control performance of the predictive model. As experimental results show, the proposed three-vector model predictive torque control can obtain small torque ripple and current harmonics both in steady state and dynamic state.

1. INTRODUCTION

Permanent magnet synchronous motors have high power density and high efficiency [1]. With the development of industrial control, there are three main control strategies for permanent magnet synchronous motors in the control field: Vector Control (VC) [2], Direct Torque Control (DTC) [3], and Model Predictive Control (MPC) [4, 5].

According to different control objectives, model predictive control can be divided into model predictive current control (MPCC) and model predictive torque control (MPTC) [6, 7]. Compared with MPCC controlling the torque indirectly by controlling the current, MPTC directly takes control with an intuitive and simple system. This article focuses its research on MPTC.

MPTC model predictive torque control is divided into single vector [8], double vector [9], and three vectors [11–14] according to the number of voltage vectors acting in a single control cycle. Single vector control is simple, but with larger torque ripple. The dual vectors improve its system performance, yet cannot meet the higher requirements for torque and flux control [10]. This article focuses on three-vector MPTC.

Traditional MPTC predicts the torque and flux linkage at the next moment and selects the optimal voltage vector combination to act on the inverter in the principle of minimum cost function [11, 12]. Although this method is simple to control, it has shortcomings. Ref. [11] makes 7 predictions in one sampling period, which requires a lot of computational costs. Some studies have proposed the optimal duty cycle MPTC method, which incorporates the voltage vector and action time into the prediction process at the same time [13, 14]. However, there is no definite general calculation design theory for the weight coefficient of flux linkage and torque. In practical applications, a large number of experiments and simulations are needed to determine the weight coefficient.

Therefore, some researchers consider eliminating the weight coefficient. Ref. [15] proposes a value function without weight coefficient based on the principle of deadbeat synchronization of torque and flux linkage on the basis of three vectors, which only includes torque as a variable, but its calculation amount

Received 4 December 2021, Accepted 13 March 2022, Scheduled 9 April 2022

* Corresponding author: Yang Zhang (hut_zy@163.com).

[1] Hunan University of Technology, Zhuzhou 412007, China. [2] CSG Electric Power Research Institute Co. Ltd, Guangzhou 510663, China.

is large. Ref. [16] proposes a three-vector improved MPTC control strategy based on an extended control set, but the controller bears more computational burden. Ref. [17] calculates the first vector by the predicted values of six effective vectors and then, based on its effective sector, calculates the second effective vector through the enumeration method. However, it also requires a large calculation.

During operation, when load changes suddenly, motor will lose balance between electromagnetic torque and load torque, causing a certain lag in speed adjustment. Ref. [18] constructs a second-order sliding mode observer to observe the disturbance caused by parameter mismatch, but the chattering caused by the switching function is difficult to eliminate. Ref. [19] uses a reduced-order Luenberger observer to estimate the load torque of the system. This structure is relatively simple and easy. Therefore, this paper introduces a reduced-order Luenerger observation compensation model to compensate for the influence of load disturbance on the control performance of the predictive model.

Considering above-mentioned problems, this paper proposes an improved three-vector MPTC control strategy for PMSM. In the principle of torque and flux linkage deadbeat synchronization, the duration of the three voltage vectors in one cycle is calculated. The 6 candidate vectors in the traditional torque prediction are reduced to two, and the optimal voltage vector is selected according to the principle of minimizing the cost function. In addition, load disturbance observation compensation is introduced to improve the sensitivity of model predictive torque control. The experiment results prove the correctness and effectiveness of the control method proposed in this paper.

2. SPMSM MODEL

This article takes the surface-mounted PMSM as the specific object. It is assumed that the stator three-phase windings are symmetrical and connected in a star shape, and the core loss is ignored. The rotor has no damper winding. Under ideal assumptions, the simplified voltage equation is [20]:

$$\begin{bmatrix} u_\alpha \\ u_\beta \end{bmatrix} = \begin{bmatrix} R_s & 0 \\ 0 & R_s \end{bmatrix} \begin{bmatrix} i_\alpha \\ i_\beta \end{bmatrix} + p \begin{bmatrix} \psi_\alpha \\ \psi_\beta \end{bmatrix} \tag{1}$$

The flux linkage equation is

$$\begin{bmatrix} \psi_\alpha \\ \psi_\beta \end{bmatrix} = \begin{bmatrix} L_s & 0 \\ 0 & L_s \end{bmatrix} \begin{bmatrix} i_\alpha \\ i_\beta \end{bmatrix} + \begin{bmatrix} \cos\theta & 0 \\ 0 & \sin\theta \end{bmatrix} \begin{bmatrix} \psi_f \\ \psi_f \end{bmatrix} \tag{2}$$

The electromagnetic torque equation is

$$T_e = \frac{3}{2} p_n (\psi_\alpha i_\beta - \psi_\beta i_\alpha) \tag{3}$$

where u_α, u_β, i_α, i_β, ψ_α, ψ_β are α and β axis stator voltages, stator currents, and stator flux linkages, respectively. The inductance value of the surface mount permanent magnet synchronous motor is $L_d = L_q = L_s$; ψ_f is the permanent magnet flux linkage; R_s is the resistance of the three-phase stator winding; p is the differential operator; θ is the rotor position angle.

The voltage equation of PMSM in the two-phase rotating coordinate system can be expressed as

$$\begin{bmatrix} u_d \\ u_q \end{bmatrix} = \begin{bmatrix} R_s & 0 \\ 0 & R_s \end{bmatrix} \begin{bmatrix} i_d \\ i_q \end{bmatrix} + \omega \begin{bmatrix} -\psi_d \\ \psi_q \end{bmatrix} + p \begin{bmatrix} \psi_d \\ \psi_q \end{bmatrix} \tag{4}$$

The flux linkage equation is

$$\begin{bmatrix} \psi_d \\ \psi_q \end{bmatrix} = \begin{bmatrix} L_s & 0 \\ 0 & L_s \end{bmatrix} \begin{bmatrix} i_d \\ i_q \end{bmatrix} + \begin{bmatrix} \psi_f \\ 0 \end{bmatrix} \tag{5}$$

The electromagnetic torque equation is

$$T_e = \frac{3}{2} p_n \psi_f i_q \tag{6}$$

In the formula, u_d, u_q, i_d, i_q, ψ_d, ψ_q are the straight axis and quadrature axis stator voltages, stator currents, and stator flux linkages, respectively; ω is the electrical angular velocity.

3. IMPROVED MODEL PREDICTIVE TORQUE CONTROL

The three-vector MPTC strategy uses three voltage vectors in one sampling period and calculates the action time of each voltage vector through the principle of torque and flux linkage deadbeat control. On this basis, it is proposed to reduce the number of candidate vectors by judging the predicted torque and flux linkage to reduce the computational burden and further reduce the harmonics of the current. The strategy can be divided into three parts: voltage vector combination selection, duration of each voltage vector in a cycle, cost function design, and switching pulse generation.

3.1. Voltage Vector Combination Selection

The three-vector-based MPTC includes three voltage vectors in one sampling period, two of which are valid and one zero vector. The method used in this paper does not need to calculate in advance, and two effective vectors are selected at the same time by judging the sector where the predicted value is located, which reduces the amount of calculation. The first-order Euler discretization of Eqs. (4) and (6) shows that:

$$i_q(k+1) = \left(1 - \frac{R_s T_s}{L_s}\right) i_q(k) - \frac{T_s}{L_s}\omega_e L_d i_d(k) - \frac{T_s}{L_s}\omega_e \psi_f + \frac{T_s}{L_s} u_q(k) \tag{7}$$

$$u_q(k+1) = \frac{L_s}{T_s}\left(\frac{T_{e\_ref}}{1.5 P_n \psi_f} - A\right) \tag{8}$$

To simplify the formula, make $A+u_q(k)T_s/L_s = i_q(k+1)$ and $B = u_q(k+1)$. According to Eqs. (1), (7) and (8):

$$u_\beta = u_\alpha \tan\theta + B/\cos\theta \tag{9}$$

The improved three-vector MPTC proposed in this paper can select the first vector and second vector at the same time according to Eq. (9), satisfying the requirement of increasing the torque to increase the flux linkage, increasing the torque to reduce the flux linkage, and reducing the torque to decrease the four control requirements of flux linkage and reducing torque to increase flux linkage which are shown in the vector combination selection table in Table 1. Taking $\tan\theta \in [0, \sqrt{3}]$ and $B/\cos\theta > 0$ as an example, the first candidate vector and second candidate vector will be selected from u_2, u_3, u_4, and the third voltage vector is a zero vector. The two combinations are (u_3, u_4), (u_3, u_2). Taking (u_3, u_4, u_7) as an example, the voltage vector synthesized by (u_3, u_4) can change the direction of the voltage vector, and the zero vector can adjust the magnitude of the voltage vector. In the same way, the direction and amplitude of the voltage vector synthesized by other combinations are adjustable, and the selectable voltage vector range after the combination of the two voltage vectors covers the shaded area in Fig. 1.

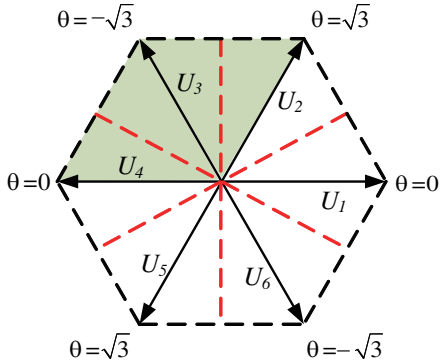

Figure 1. Schematic diagram of improved MPTC selectable voltage vector range.

Table 1. Vector combination selection table.

$\tan\theta$	$B/\cos\theta$	Combination selection
$[0,\sqrt{3}]$	>0	$u_{2,3,4}$
$[0,\sqrt{3}]$	<0	$u_{1,5,6}$
$\sqrt{3},+\infty]$	>0	$u_{1,2,6}$
$\sqrt{3},+\infty]$	<0	$u_{3,4,5}$
$(-\sqrt{3},0]$	>0	$u_{1,2,3}$
$(-\sqrt{3},0]$	<0	$u_{1,5,6}$
$[-\infty,-\sqrt{3}]$	>0	$u_{1,2,6}$
$[-\infty,-\sqrt{3}]$	<0	$u_{3,4,5}$

3.2. Time Distribution of the Voltage Vector

After selecting the voltage vector combination, it is necessary to allocate the respective action time of the three vectors in a control cycle. This paper uses the deadbeat control method of torque and flux linkage to calculate. The voltage vector action diagram is shown in Fig. 2.

$$\begin{cases} S_{T_{e\_out1}} = \dfrac{T_e(k+1)_{out1} - T_e(k)}{T_s} \\ S_{\psi_{s\_out1}} = \dfrac{\psi_s(k+1)_{out1} - \psi_s(k)}{T_s} \\ S_{T_{e\_out2}} = \dfrac{T_e(k+1)_{out2} - T_e(k)}{T_s} \\ S_{\psi_s\_out2} = \dfrac{\psi_s(k+1)_{out2} - \psi_s(k)}{T_s} \\ S_{T_e\_out3} = \dfrac{T_e(k+1)_{out3} - T_e(k)}{T_s} \\ S_{\psi_s\_out3} = \dfrac{\psi_s(k+1)_{out3} - \psi_s(k)}{T_s} \end{cases} \tag{10}$$

In the formula, $T_e(k+1)_{out1}$, $T_e(k+1)_{out2}$, $T_e(k+1)_{out3}$, $\psi_s(k+1)_{out1}$, $\psi_s(k+1)_{out2}$, and $\psi_s(k+1)_{out3}$ are the predicted values of torque and flux linkage under the action of the first, second, and third voltage

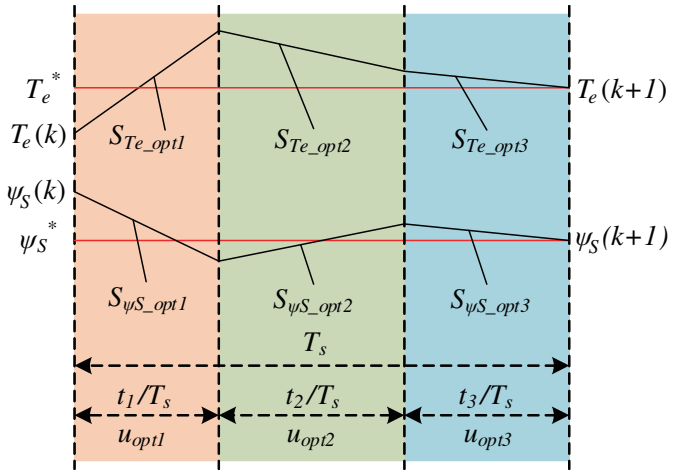

Figure 2. Diagram of voltage vector action.

vectors u_{out1}, u_{out2}, and u_{out3}, respectively. $T_e(k)$ and $\psi_s(k)$ are the torque value and flux linkage value at the current moments.

The torque and flux linkage adopt deadbeat control, so that the predicted values of the torque and flux linkage reach the given value $T_{e\_ref}(k)$ and $\psi_{s\_ref}(k)$ in one cycle, that is, it satisfies:

$$\begin{cases} T_e(k+1) = T_{e\_ref} = T_e(k) + S_{T_{e\_out1}} t_1 + S_{T_{e\_out2}} t_2 + S_{T_{e\_out3}} t_3 \\ |\psi_s(k+1)| = \psi_{s\_ref} = |\psi_s(k)| + S_{\psi_{s\_out1}} t_1 + S_{\psi_{s\_out2}} t_2 + S_{\psi_{s\_out3}} t_3 \end{cases} \tag{11}$$

In the formula, $t_3 = T_s - t_1 - t_2$; T_{e_ref} and ψ_{s_ref} are the given values of torque and flux linkage.

After calculating the action time of the three voltage vectors, to ensure that t_1, t_2, and t_3 are within the range of $0 \sim T_s$, it is necessary to judge the action time, as follows:

1) When any two of the action times t_1, t_2, and t_3 have an action time less than 0, and the other action time is greater than T_s, let the action time less than 0 be equal to 0, and the action time greater than T_s should be equal to T_s.

2) When any two action times (t_a, t_b) of action times t_1, t_2, and t_3 are greater than zero, and the other action time t_c is less than 0, it is necessary to perform overmodulation processing on the three action times, namely:

$$\begin{cases} t_{a\_1} = \dfrac{t_a T_s}{t_a + t_b} \\ t_{b\_1} = \dfrac{t_b T_s}{t_a + t_b} \\ t_{c\_1} = 0 \end{cases} \tag{12}$$

In the formula, t_a and t_b are the action times of any of t_1, t_2, and t_3 greater than 0; t_c is the action time of t_1, t_2 and t_3 less than 0; t_{a_1}, t_{b_1}, and t_{c_1} are the action times of the three voltage vectors after correction.

3.3. Cost Function Design

The value function in the traditional MPTC generally includes two physical quantities of different dimensions, torque and flux linkage, so weight coefficients need to be introduced. The expression of the value function is:

$$g = \lambda(T_{e\_ref} - T_e(k+1))^2 + (\varphi_{s\_ref} - \varphi_s(k+1))^2 \tag{13}$$

In the formula, λ is the weight coefficient.

Since there is no corresponding formula for the weight coefficient to be calculated, in many papers, it is collected through empirical trials, and the size of the weight coefficient will directly affect the system performance. The method adopted in this paper adopts the deadbeat control of torque and flux linkage. When the torque reaches the given value, it also ensures that the flux linkage reaches the given value. Therefore, the value function can be designed as:

$$g = |T_e(k+1) - T_{e\_ref}| \tag{14}$$

The main steps of improving the three-vector model predictive torque control are as follows:

1) Obtain the currents i_d, i_q at time k, and collect the rotor position at the current time;

2) Determine the voltage vector combination through the voltage vector combination selection in Section 3.1, and calculate the respective action times under the action of the three voltage vectors in the two voltage vector combinations;

3) Calculate the predicted values of torque and flux linkage under the two voltage vector combinations, and calculate the corresponding cost functions of the two voltage vector combinations according to Eq. (14);

4) Select a set of voltage vectors that minimizes the cost function and its corresponding action time to act on the inverter.

3.4. Design of Disturbance Observer

The load disturbance observer adopts the reduced-order Luenberger load observer to estimate the load torque of the system. Compared with the full-order observer, its structure is simpler.

According to Eq. (3), the kinematics equation of the motor can be rewritten as:

$$\begin{cases} \dfrac{d\widehat{\omega}_r}{dt} = -\dfrac{B}{J}\omega_r - \dfrac{1}{J}\widehat{T}_L + h_1(\omega_r - \widehat{\omega}_r) \\ \dfrac{d\widehat{T}_L}{dt} = h_2(\omega_r - \widehat{\omega}_r) \end{cases} \tag{15}$$

The motor quadrature axis current i_q and rotor speed ω_r are used as input, and the observed torque $\hat{T}_L$ and the observed quadrature axis current $\hat{i}_q$ are used as output variables. At this time, a reduced-order Luenberger observer is formed.

In the control system, the state observer realizes digital control by means of discrete recursion. Assuming that the sampling period of the speed loop of the system is T_s, the discretization of Eq. (15) can obtain the recursive formula of the observed value of speed and load torque as:

$$\begin{cases} \hat{\omega}_r(k+1) = (1 - Th_1)\hat{\omega}_r(k) + T\left(h_1 - \dfrac{B}{J}\right)\omega_r(k) + \dfrac{Tk}{J}i_q(k) - \dfrac{T}{J}\hat{T}_L(k) \\ \hat{T}_L(k+1) = \hat{T}_L(k) + Th_2\ [\omega_r(k) - \hat{\omega}_r(k)] \end{cases} \tag{16}$$

The schematic diagram of the structure of the reduced-order Lemberg observer is shown in Fig. 3. It can be seen that the input of the observer is the motor speed and torque current command value, and the output is the observed load torque.

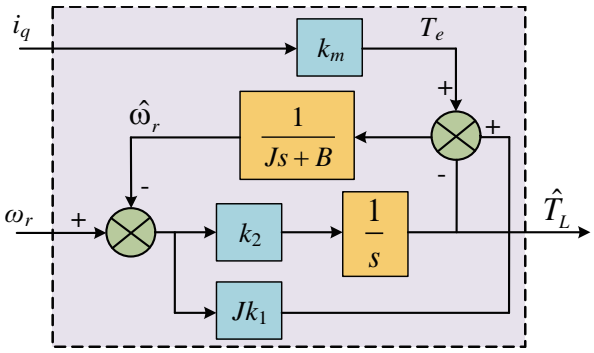

Figure 3. Block diagram of reduced order Luenberger observer.

The load torque observed by the reduced-order Luenberger observer is fed forward and compensated to the torque reference output by the speed loop as a compensation signal for load disturbance. The compensated torque prediction controller can be obtained from Eq. (11) The torque command value is:

$$T_e(k+1) = T_e(k) + S_{T_{e\_out1/2/3}}t_{1/2/3} + T_L \tag{17}$$

The control block diagram of the PMSM system is shown in Fig. 4. In the figure, the inner loop of the current adopts the improved dead-beating torque prediction control method, and the outer loop of the speed adopts the PI control method with the introduction of the reduced-order Luenberger observer, which constitutes the improved MPTC control system with the introduction of observation compensation.

3.5. Pulse Generation

According to the principle of minimum cost function in Section 3.3 of this paper, three combinations of voltage vectors and their respective action time synthesis vectors u_{opt} are selected, and the given voltage

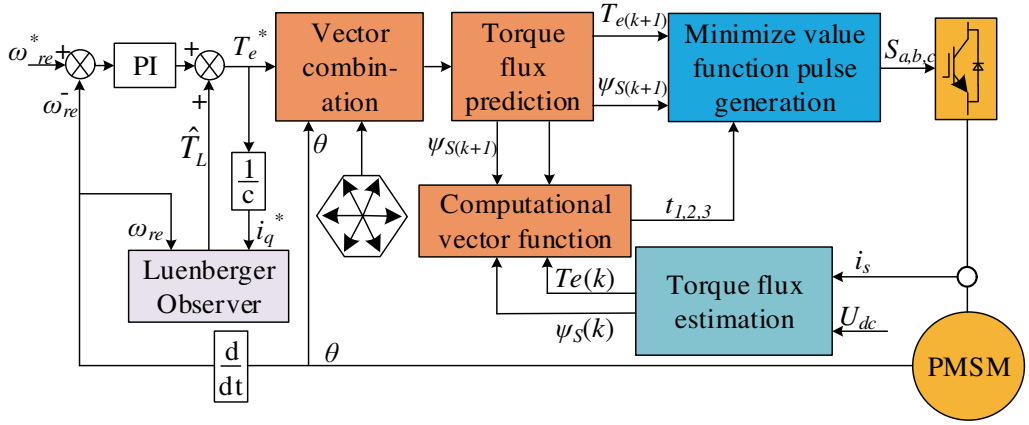

Figure 4. Structure block diagram of improved MPTC control system with Luenberger observation compensation.

vector is synthesized by SVM (Support Vector Machine). This method can ensure the constant switching frequency and improve the steady-state performance of the system without significantly increasing the calculation amount of the control strategy. This article uses a seven-segment SVM to synthesize a given voltage vector.

The magnitude and position of the given voltage vector can determine the two adjacent effective voltage vectors in the corresponding sector and their action time. From this, the action time of the zero vector is obtained. According to the principle of "volt-second balance", as shown in Fig. 5 (take the first sector as an example), after the action time of the two effective voltage vectors is divided equally, they are inserted between the zero vectors. According to the principle of minimum switching loss, the middle the zero voltage vector is U_7, which effectively reduces the harmonic components of Pulse Width Modulation (PWM).

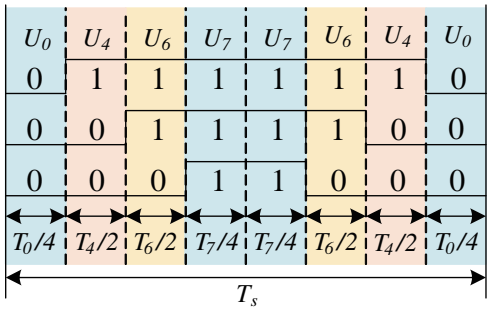

Figure 5. Seven-segment SVM.

4. EXPERIMENTAL ANALYSIS

In this paper, the proposed improved torque predictive control algorithm and the control method used in the literature [17] are respectively verified by experiments, and a hardware platform based on TI digital processor TMS320F28335 is built, as shown in Fig. 6(a)), in which **I** is the control cabinet, which is used for algorithm verification; **II** is the isolation transformer; **III** is the upper computer for storing and displaying output data; **IV** is the DC brushless motor, which realizes loading and unloading; **V** is the torque signal acquisition module; **VI** is the control motor. The circuit of the control cabinet is shown in Fig. 6(b), in which 1 is the PMSM power driver module; 2 is the load DC motor power drive module; 3 is the dc power supply module with stable voltage; 4 is the sampling circuit; 5 is the TMS320F28335 core control board. The experimental motor parameters are shown in Table 2.

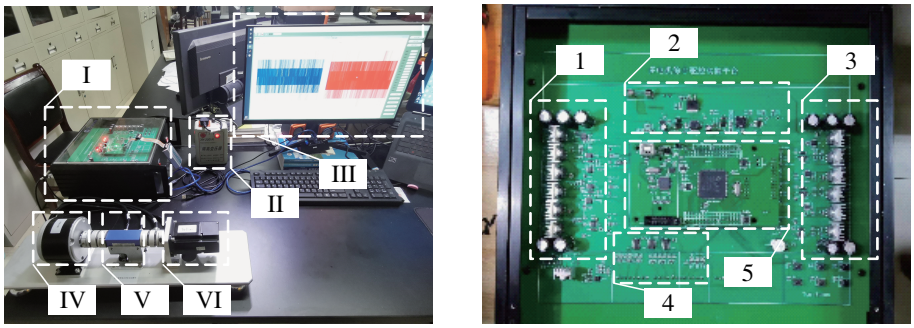

(a) (b)

Figure 6. Hardware platform based on TI digital processor TMS320F28335.

Table 2. PMSM parameters.

Parameter	Symbol	Value
Rated power	P	200 W
Permanent magnet flux	Ψ_f	0.0105 Wb
Stator inductance	L_s	0.9 mH
Stator resistance	R_s	0.33 Ω
Rated torque	T_N	0.637 Nm
Rated speed	N	3000 r/min
Inertia	J	0.0096 Kg · m^2
Number of pole pairs	P_n	4

The experiment in this paper mainly studies the improvement of the calculation amount of the system. In order to avoid the influence of the speed loop PI parameters on the system performance, the speed outer loops all use the same PI parameters ($K_p = 0.004$, $K_i = 0.0008$).

4.1. Improved Algorithm Comparison Experiment

The total running time of the system is 30.0 s. After the program is started, the PMSM starts up to the speed of 1500 r/min without load at 10 s, adds a sudden load of 0.12 Nm at 15 s, and unloads at 20 s. The speed waveform of PMSM with two control modes of three-vector MPTC and improved three-vector MPTC is shown in Fig. 7. It can be seen from Table 3 that the start-up time of the two control methods is about 0.18 s, and the speed response is relatively rapid. When the load changes suddenly, the speed fluctuations of the two control strategies quickly return to the given value. The improved three-vector MPTC reduces the number of candidate vectors from 6 to 2, which reduces the computational burden of the system. According to the experimental results, it can be seen that the improvement of the algorithm does not affect the fast dynamic response of predictive control.

Figure 8 shows the torque output waveforms of the two control modes PMSM when the motor is loaded and unloaded. It can be seen from Table 4 that the maximum range of torque ripple of the improved three-vector MPTC algorithm is 0.13, which is 13.3% smaller than that of the traditional MPTC algorithm, which is 0.15. In the 16 s $\sim$ 19 s time period after loading steady state, the torque ripple root mean square of the improved three-vector MPTC algorithm is 0.115, which is 2.5% lower than that of the traditional MPTC algorithm, which is 0.119. Compared with the traditional MPTC algorithm, the improved MPTC control strategy can accurately judge the predicted value of torque and flux linkage prediction by using formula (9) and effectively reduce the torque ripple.

Figure 9 shows the waveforms of the A-phase output current of the two control modes PMSM in the 17.3 s $\sim$ 17.8 s period after the motor is stably loaded. The given speed of the motor is 1500 r/min,

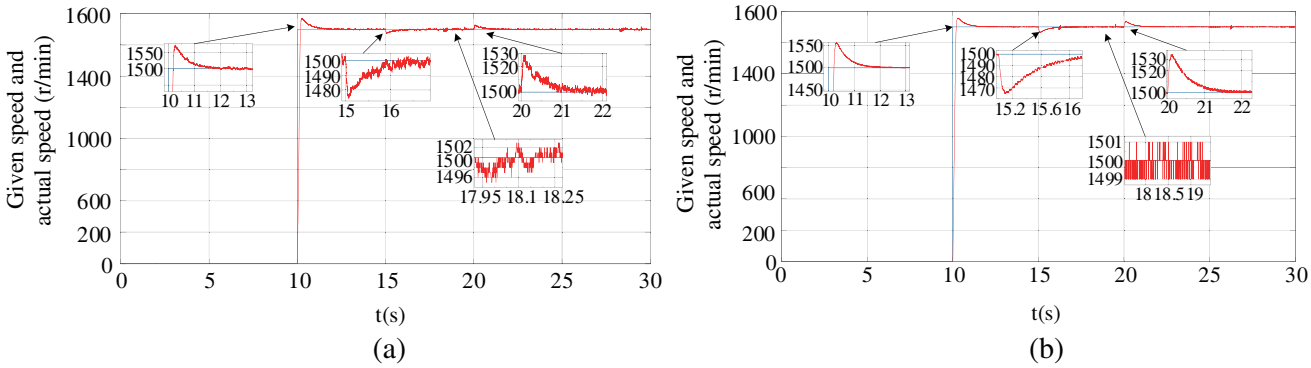

Figure 7. The experimental waveforms of the rotational speed when the two control strategies are loaded and unloaded. (a) Three vector MPTC. (b) Improved three-vector MPTC.

Table 3. Comparison of speeds of the two control strategies.

Parameter	Three vector MPTC	Improved three-vector MPTC
Δs (s)	0.18	0.2
Δn (r/min)	2	1
$\Delta n1$ (r/min)	26	35
$\Delta n2$ (r/min)	29	35
$t1$ (s)	1.35	1.43
$t2$ (s)	0.87	1.35

(Δs: start-up time, that is, the time for the motor to reach a given speed from zero speed; Δn: speed error at steady state; $\Delta n1$: maximum speed drop value when the sudden load is applied; $\Delta n2$: maximum speed rise value during unloading; $t1$: time to steady state after sudden load; $t2$: Time to steady state after sudden load).

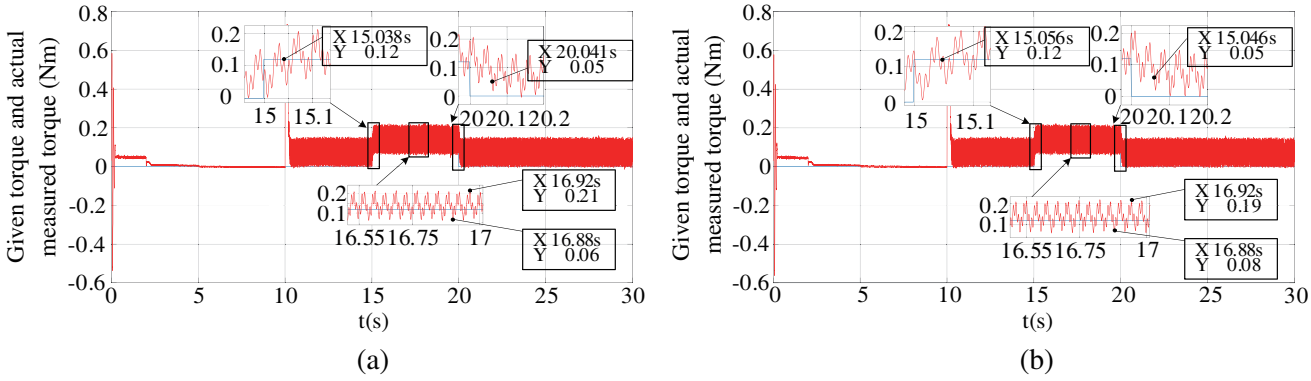

Figure 8. Torque experimental waveforms of two control strategies during loading and unloading. (a) Three vector MPTC. (b) Improved three-vector MPTC.

and it can be seen from Fig. 10 that the fundamental frequency of the motor is 100 Hz. It can be seen from Table 5 that the current harmonic using the improved MPTC algorithm is 6.22%, compared with 13.86% for the traditional MPTC control strategy, and the reduction ratio is 55.12%. The reduction of current harmonics is also the key reason for the reduction of torque output ripple. From the FFT analysis in Fig. 9, the traditional MPTC algorithm harmonics are mainly the third and fifth harmonics. The improved three-vector MPTC control strategy effectively reduces the third and fifth harmonics of the current, and the reduction ratios are 57.2% and 84.9%.

Table 4. Torque comparison of the two control strategies.

Parameter	Three vector MPTC	Improved three-vector MPTC
$\Delta Temin(Nm)$	0.06	0.04
$\Delta Temax(Nm)$	0.09	0.07
$\Delta Te1(ms)$	38	56
$\Delta Te2(ms)$	41	46

($\Delta Te_{\min}$ is the minimum torque fluctuation during loading;
$\Delta Te_{\max}$ is the maximum torque fluctuation during loading;
$\Delta Te1$ is the torque response time from the moment of loading to when the torque is stable;
$\Delta Te2$ 123 is the torque response time from the moment of unloading to when the torque is stable).

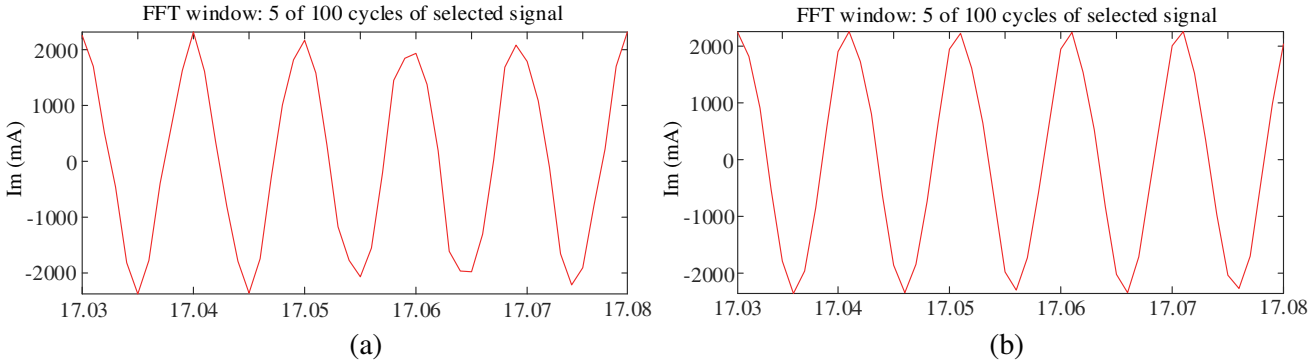

Figure 9. Experimental waveforms of motor phase A current of two control strategies. (a) Three vector MPTC. (b) Improved three-vector MPTC.

4.2. Introduce Observation Compensation Experiment

The total running time of the system is 30.0 s. After the program is started, the PMSM starts at no-load to 1500 r/min at 10 s, adds a sudden load of 0.12 Nm at 15 s, and unloads at 20 s. Based on the observation of feedforward compensation, after adopting the improved three-vector MPTC control strategy, the PMSM speed waveform is shown in Fig. 11(a). The waveform of the A phase output current of the PMSM during the 17.3 s $\sim$ 17.8 s period is shown in Fig. 11(b). The given speed of the motor is 1500 r/min, and it can be seen from Fig. 11(d) that the fundamental frequency of the motor is 100 Hz. It can be seen from Table 5 that the Total Harmonic Distortion (THD) of the control strategy of the improved MPTC algorithm with observation feedforward is 9.58%, which is 3.36% higher than

Table 5. Experimental data of introducing disturbance compensation.

Parameter	Improved three-vector MPTC	Improved three-vector MPTC + feedforward compensation
Δs (s)	.2	.2
Δn (r/min)	1	2
$\Delta n1$ (r/min)	35	13
$\Delta n2$ (r/min)	35	11
$t1$ (s)	1.43	1.02
$t2$ (s)	1.35	1.08
THD (%)	6.22	9.58

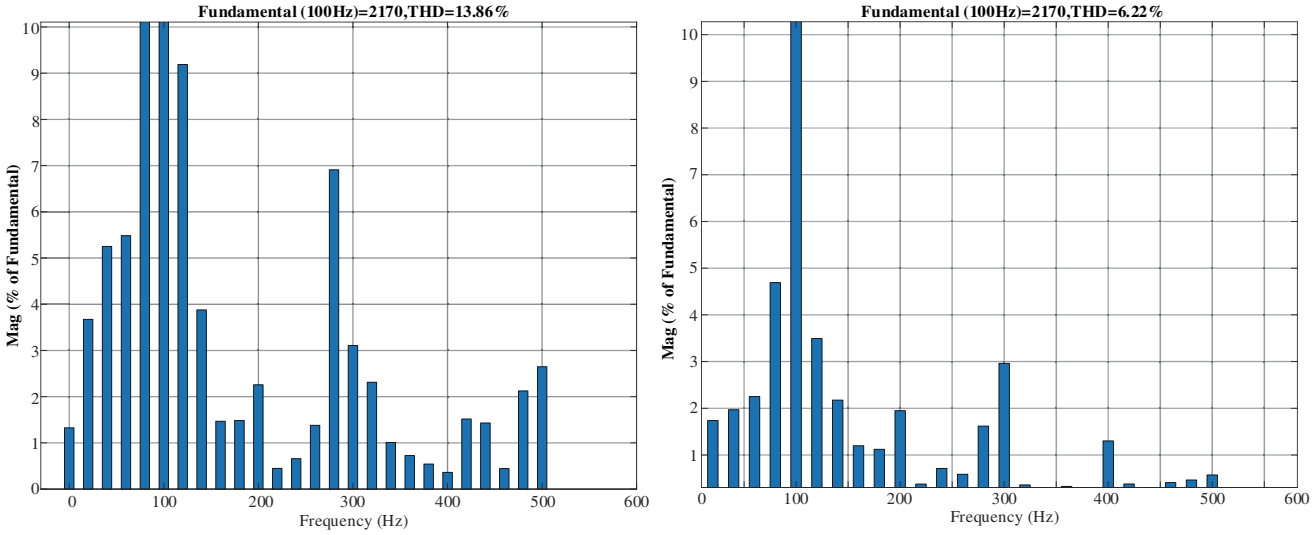

Figure 10. FFT spectrum analysis of permanent magnet synchronous motor with two strategies. (a) Three vector MPTC. (b) Improved three-vector MPTC.

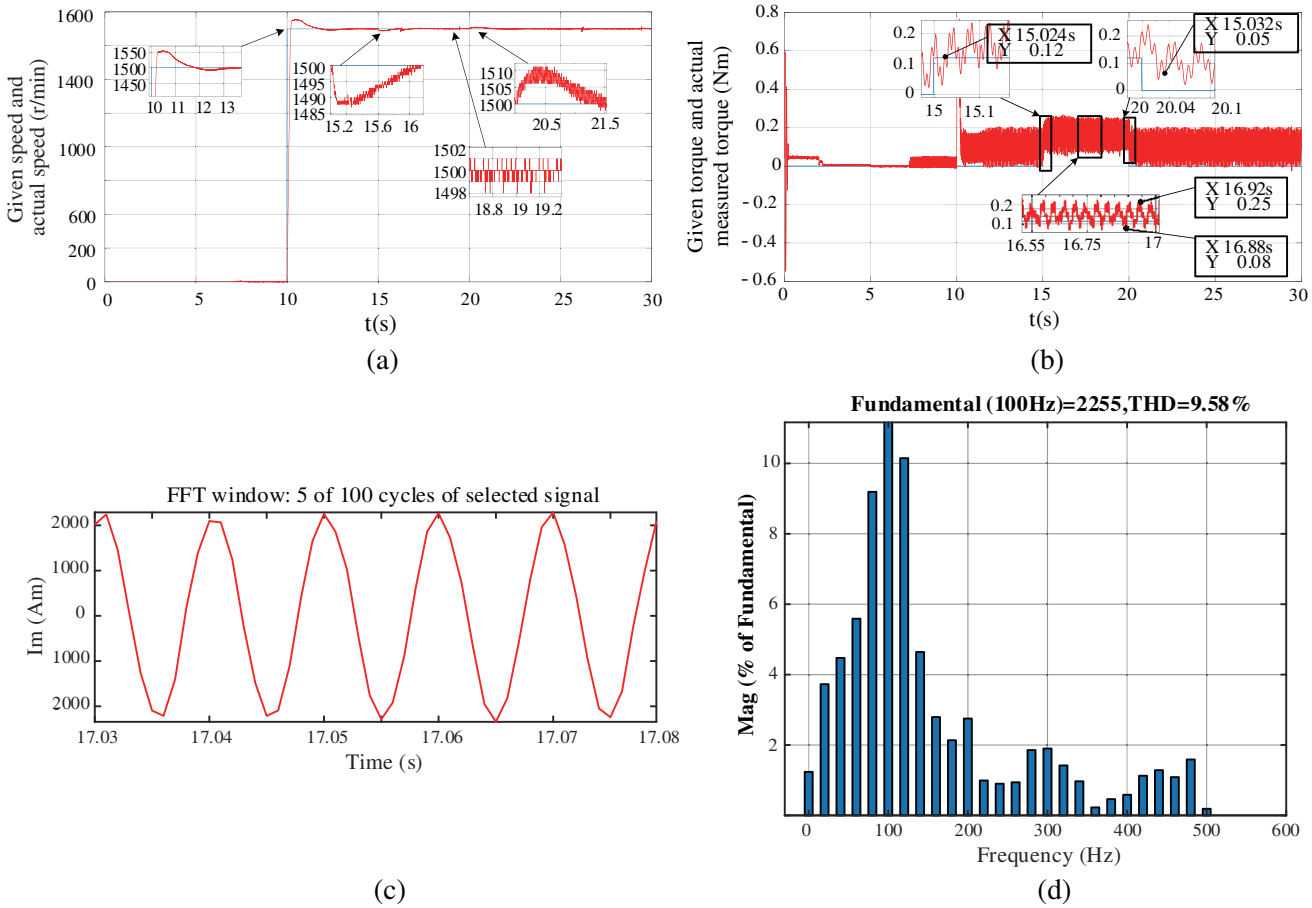

Figure 11. Improved MPTC + observation feedforward compensation experimental waveform. (a) Motor speed waveform. (b) Torque experimental waveforms. (c) Motor phase A current waveform. (d) FFT spectrum analysis diagram of motor phase A current.

that of the improved MPTC algorithm, but 30.88% lower than that of the traditional MPTC algorithm. It can be seen from Fig. 11(a) that the introduction of compensation can effectively improve the anti-interference performance of the motor. Compared with the improved MPTC control strategy, the sudden load speed drop and the unloaded speed change are reduced by 22 r/min and 24 r/min, respectively. It effectively reduces the large changes in the motor speed due to load disturbances.

It can be seen from Fig. 11(b) that in the 16 s $\sim$ 19 s time period after loading steady state, the torque ripple root mean square of the improved three-vector MPTC algorithm with observation compensation is 0.12, which is larger than that of the improved MPTC algorithm. However, the torque response speed of the improved three-vector MPTC algorithm with observation compensation is 14 ms faster than that of the improved MPTC, which effectively improves the dynamic response speed of the motor.

5. CONCLUSION

Based on the three-vector predictive control strategy of permanent magnet synchronous motor, the effect of voltage vector combination on the system stability is studied, and the compensation technique of disturbance observation is introduced to compensate the effect of load disturbance on the predictive model control performance. The following conclusions are drawn from the experimental results:

1) By judging the combination of voltage vectors and selecting the combination mode of voltage vectors, it is not necessary to calculate the action time of the first voltage vector before calculating the action time of the other two vectors, which reduces the computational burden of the system. The improved MPTC control strategy not only reduces the torque ripple, but also reduces the current harmonics by 7.64% compared with the traditional MPTC control strategy;

2) After introducing observation compensation based on the improved MPTC control strategy, the torque response speed is improved, and the large change in motor speed caused by load disturbance is reduced. The introduction of observation compensation can effectively speed up the dynamic response of the improved MPTC control strategy to load changes.

ACKNOWLEDGMENT

This work was supported by the National Natural Science Foundation of China under Grant Number 51907061, Educational Commission of Hunan Province of China under Grant Number 21B0552, and National Engineering Laboratory of UHV Engineering Technology under Grant Number NEL202008.

REFERENCES

1. Ding, X., J. Cheng, Z. Zhao and P. Chi Kwong Luk, "A high-precision and high-efficiency PMSM driver based on power amplifiers and RTSPSs," *IEEE Transactions on Power Electronics*, Vol. 36, No. 9, 10470–10480, Sept. 2021, doi: 10.1109/TPEL.2021.3063312.
2. Wang, W., et al., "New three-phase current reconstruction for PMSM drive with hybrid space vector pulsewidth modulation technique," *IEEE Transactions on Power Electronics*, Vol. 36, No. 1, 662–673, Jan. 2021, doi: 10.1109/TPEL.2020.2997986.
3. Zhang, X. and Y. He, "Direct voltage-selection based model predictive direct speed control for PMSM drives without weighting factor," *IEEE Transactions on Power Electronics*, Vol. 34, No. 8, 7838–7851, Aug. 2019, doi: 10.1109/TPEL.2018.2880906.
4. Tong, W., S. Dai, S. Wu and R. Tang, "Performance comparison between an amorphous metal PMSM and a silicon steel PMSM," *IEEE Transactions on Magnetics*, Vol. 55, No. 6, 1-5, Jun. 2019, Art No. 8102705, doi: 10.1109/TMAG.2019.2900531.
5. Sun, X., Z. Shi, G. Lei, Y. Guo and J. Zhu, "Analysis and design optimization of a permanent magnet synchronous motor for a campus patrol electric vehicle," *IEEE Transactions on Vehicular Technology*, Vol. 68, No. 11, 10535–10544, Nov. 2019, doi: 10.1109/TVT.2019.2939794.

6. Siami, M., D. A. Khaburi, A. Abbaszadeh and J. Rodríguez, "Robustness improvement of predictive current control using prediction error correction for permanent-magnet synchronous machines," *IEEE Transactions on Industrial Electronics*, Vol. 63, No. 6, 3458–3466, Jun. 2016, doi: 10.1109/TIE.2016.2521734.
7. Zhao, G., J. Feng and Q. Sun, "The research of optimized torque control algorithm for PMSM based on grey prediction model," *2009 Sixth International Conference on Fuzzy Systems and Knowledge Discovery*, 335–340, 2009, doi: 10.1109/FSKD.2009.588.
8. Chen, W. and D. Sun, "A simplified robust model predictive flux control of open-winding PMSM based on ESO," *2019 22nd International Conference on Electrical Machines and Systems (ICEMS)*, 1–6, 2019, doi: 10.1109/ICEMS.2019.8921676.
9. Zhang, X., K. Yan, and M. Cheng, "Two-stage series model predictive torque control for PMSM drives," *IEEE Transactions on Power Electronics*, Vol. 36, No. 11, 12910–12918, Nov. 2021, doi: 10.1109/TPEL.2021.3075711.
10. Ji, J., R. Xue, W. Zhao, T. Tao, and L. Huang, "Simplified three-vector-based model predictive thrust force control with cascaded optimization process for a double-side linear vernier permanent magnet motor," *IEEE Transactions on Power Electronics*, Vol. 35, No. 10, 10681–10689, Oct. 2020, doi: 10.1109/TPEL.2020.2976901.
11. Yan, L., M. Dou, Z. Hua, H. Zhang, and J. Yang, "Robustness improvement of FCS-MPTC for induction machine drives using disturbance feedforward compensation technique," *IEEE Transactions on Power Electronics*, Vol. 34, No. 3, 2874–2886, Mar. 2019, doi: 10.1109/TPEL.2018.2842743.
12. Wu, M., X. Sun, J. Zhu, G. Lei, and Y. Guo, "Improved model predictive torque control for PMSM drives based on duty cycle optimization," *IEEE Transactions on Magnetics*, Vol. 57, No. 2, 1–5, Feb. 2021, Art No. 8200505, doi: 10.1109/TMAG.2020.3008495.
13. Nikzad, M. R., B. Asaei, and S. O. Ahmadi, "Discrete Duty-Cycle-Control method for direct torque control of induction motor drives with model predictive solution," *IEEE Transactions on Power Electronics*, Vol. 33, No. 3, 2317–2329, Mar. 2018, doi: 10.1109/TPEL.2017.2690304.
14. Woldesemayat, M. L., H. Lee, S. Won, and K. Nam, "Modeling and verification of a six-phase interior permanent magnet synchronous motor," *IEEE Transactions on Power Electronics*, Vol. 33, No. 10, 8661–8671, Oct. 2018, doi: 10.1109/TPEL.2017.2782804.
15. Bhaumik, A. and S. Das, "Predictive torque control scheme without weighting factors for speed sensorless induction motor drive," *2021 1st International Conference on Power Electronics and Energy (ICPEE)*, 2021, 1–6, doi: 10.1109/ICPEE50452.2021.9358475.
16. Sun, X., et al., "MPTC for PMSMs of EVs with multi-motor driven system considering optimal energy allocation," *IEEE Transactions on Magnetics*, Vol. 55, No. 7, 1–6, Jul. 2019, Art No. 8104306, doi: 10.1109/TMAG.2019.2904289.
17. Chen, L., H. Xu, X. Sun, and Y. Cai, "Three-vector-based model predictive torque control for a permanent magnet synchronous motor of EVs," *IEEE Transactions on Transportation Electrification*, Vol. 7, No. 3, 1454–1465, Sept. 2021, doi: 10.1109/TTE.2021.3053256.
18. Wang, B., Z. Dong, Y. Yu, G. Wang, and D. Xu, "Static-errorless deadbeat predictive current control using second-order sliding-mode disturbance observer for induction machine drives," *IEEE Transactions on Power Electronics*, Vol. 33, No. 3, 2395–2403, Mar. 2018, doi: 10.1109/TPEL.2017.2694019.
19. Wang, Y., S. Yang, and Z. Xie, "Extended state observer based current decoupling control for PMSM," *2019 22nd International Conference on Electrical Machines and Systems (ICEMS)*, 1–6, 2019, doi: 10.1109/ICEMS.2019.8921959.
20. Kim, H., J. Han, Y. Lee, J. Song, and K. Lee, "Torque predictive control of permanent-magnet synchronous motor using duty ratio prediction," *2013 IEEE International Symposium on Industrial Electronics*, 1–5, 2013, doi: 10.1109/ISIE.2013.6563664.